Catalyst Wetting Characteristics in Trickle-Bed Reactors

Arunabha Kundu and K. D. P. Nigam
Dept. of Chemical Engineering, Indian Institute of Technology, New Delhi-110016, India

R. P. Verma
Research and Development Center, Indian Oil Corporation Ltd., Faridabad-121007, India

A model for external wetting efficiency of the catalyst in trickle-bed reactors was developed based on 1-D force-balance equations incorporating drag forces in a three-phase system. The gas–liquid interfacial drag was considered, as well as the tortuosity effect. The overall model was tested with major experimental data of a 15.2-cm-dia. trickle-bed reactor using a radioisotope tracer technique. Five catalyst packings, different in shape and size, were used in the experiment. External wetting efficiency was calculated from the square root of the ratio of the effective diffusivities in two-phase and liquid-filled operation. The model was also compared with other experimental data available in the literature. The predictions were within an average confidence limit of $\pm 15\%$.

Introduction

Trickle-bed reactors are a class of multiphase reactors in which gas and liquid flow with cocurrent downward mode through a fixed bed of catalyst. These reactors are mainly used for hydroprocessing (hydrotreatment and hydrocracking) in the petroleum refining industry. Other applications are in petrochemical, biochemical, electrochemical, and waste-treatment processes. Complete understanding of the different hydrodynamic parameters in trickle-bed reactors is essential for the improvement in design and getting a better performance.

External wetting efficiency (that is, fraction of external area of catalyst effectively wetted by the liquid flowing down the bed) of the catalyst is an important feature in trickle-bed operation, as it gives an indication of the extent of catalyst utilization. It is a function of the flow rate of gas and liquid, operating pressure, physical properties of liquid, and diameter of the catalyst. In many reactions in trickle-bed reactors, one of the main reactants is nonvolatile (such as in hydroprocessing, one of the reactants is liquid and nonvolatile at the operation pressure in about all cases), so that a reaction can occur only on the wetted surface of the catalyst. In that case, partial wetting of the catalyst will decrease the reaction rate. Although at high superficial liquid velocity in the presence of the flow of gas, the external wetting efficiency of a catalyst in a commercial trickle-bed reactor should be close to unity; strictly speaking, a trickle-bed reactor deals with very low superficial liquid velocity. Consequently, external wetting efficiency of a catalyst plays a significant role in the performance of trickle-bed reactors. Moreover, poor initial distribution of liquid can cause partial wetting of the catalyst (Kundu et al., 2001). Al-Dahhan and Dudukovic (1995) and Pironti et al. (1999) reported that the external wetting efficiency will increase with the increase of superficial gas velocity due to the increase in shear stress on the gas–liquid interface, whereas Sederman and Gladden (2001) and Rucker and Akgerman (1987) showed the negligible effect of gas flow rate on wetting efficiency under the operating conditions investigated. In addition, with the very high volumetric flow ratio of gas and liquid (such as in hydroprocessing, volumetric flow of hydrogen/hydrocarbon = 500 $\sim$ 1,000) will create the dominating behavior of the gas over the catalyst particles and enhance the tendency of the liquid to bypass parts of the bed. A low value of external wetting efficiency is a major problem with pilot-scale trickle-bed reactors that are used for scaling-up and scaling-down of commercial trickle-bed reactors (Sie and Krishna, 1998; Chander et al., 2001).

In the literature, the external wetting efficiency of a catalyst in a trickle-bed reactor has been obtained from a chemical method based on reaction rates, dynamic tracer technique and dissolution, and dye adsorption technique. The dynamic tracer technique has been used by many authors (Al-Dahhan

Correspondence concerning this article should be addressed to K. D. P. Nigam.

and Dudukovic, 1995, 1996; Ring and Missen, 1991; Mills and Dudukovic, 1981), which allows the determination of wetting efficiency in actual beds under operating conditions. Llano et al. (1997) has determined the wetting efficiency using the reaction method. In reality, the reaction method requires an adequate reactor model, the main difficulty of which lies in axial dispersion. Saroha and Nigam (1996) have discussed these methods in detail. A complete review of the different methods for the measurement of wetting efficiency in a trickle-bed reactor and its different forms of definitions based on those methods has been presented by Pironti et al. (1999). In addition to their review, it is to be mentioned that there are many correlations available in the literature (for example, Ring and Missen, 1991; Larachi et al., 2001; Al-Dahhan and Dudukovic, 1995) for the prediction of external wetting efficiency in trickle-bed reactors based on the experimental results. Recently, Iliuta and Larachi (1999) and Iliuta et al. (1999) have estimated the external wetting efficiency based on a slit model (Holub et al., 1992, 1993) considering the gas–liquid interaction.

Narasimhan et al. (2002) have developed a model for the prediction of the pressure gradient and liquid holdup in trickle-bed reactors considering particle drag, particle–liquid drag, and gas–liquid interfacial drag. Their results have compared well with the experimental data available in the literature. Pironti et al. (1999) have verified their model for the wetting efficiency with experimental data that they collected at atmospheric pressure. However, with the experimental data of Al-Dahhan et al. (1995), they found that the wetting efficiency predicted by their model was greater than the one for high gas velocities (greater than 8 cm/s). They attributed this to the fact that their model did not take into account the gas–liquid interaction, which is predominantly present at high gas velocities. The gas–liquid interfacial drag becomes more significant for trickle-bed reactors operating at high pressure due to the increase of the pressure gradient. Pironti's work is significant, since it has related the wetting efficiency to the hydrodynamics of the trickle-bed reactor.

In the present article, a model for the wetting efficiency had been developed based on the physics of the fluid prevailing in the bed. The gas–liquid phase interaction term has been included in the model. For verification of the model, the radioisotope tracer technique was used to collect the experimental data in a trickle-bed reactor of 0.152 m dia. operating at atmospheric pressure. The advantages of the radioisotope tracer technique are discussed in Pant et al. (2001) and Nigam et al. (2001). The experimental value of the external wetting efficiency has been measured by the square root of the ratio between the effective diffusivity of a tracer in two phase flow and the same at liquid-full peration (single-phase flow of liquid in which the bed is fully filled with the liquid) proposed by Sicardi et al. (1980) and Mills and Dudukovic (1981). The model has also been compared with the experimental data of Al-Dahhan and Dudukovic (1995, 1996), Pironti et al. (1999), and Sederman and Gladden (2001).

Development of the Model

Assuming that the whole liquid flows as a falling film and the gas phase flows as a continuous phase in the trickle-bed reactor configuration, point-force balances are applied to the two flowing phases. Gas- and liquid-flow configurations in a unit-volume cell representing cross-sectionally averaged flow conditions are shown in Figure 1. The annular configuration has been postulated here, but such a force balance should be equally applicable to other flow regimes, provided the effect of the flow regimes is attributed elsewhere.

In the figure, particle–gas drag force, F_{PG}, is opposed by an equal and opposite force applied by the particles on the other side of the liquid layer. F_I is the drag force on the gas as a result of relative motion between the two phases (Narasimhan et al., 2002). The force balance on the gas phase is given by

$$\{(-dP/dZ)+\rho_G g\tau\}\alpha\epsilon = F_{PG} + F_I \tag{1}$$

The term α is the gas saturation, which is defined as the volume of gas present in a void volume of the reactor and can be obtained from the difference of the value of unity and the liquid saturation, β. The liquid-phase force can also be broken into two components, F_{PG} and F_{PL}. The first component, F_{PL}, is simply a reaction to the force by which the gas pushes the liquid against the particles. The second component, F_{PL}, represents the force acting on the particles due to the liquid motion. The force balance on the liquid then yields

$$\{(-dP/dZ)+\rho_L g\tau\}(1-\alpha)\epsilon = F_{PL} - F_I, \tag{2}$$

where F_{PG}, F_{PL}, and F_I represent the drag forces per unit of the total bed volume. The model for particle–liquid and particle–gas drag was obtained from the modified Kozeny-Carman equation. The model equations are elaborated in Narashimhan et al. (2002).

For a liquid-filled-bed operation, we have

$$\{(-dP/dZ)_{\text{liquid-filled bed}} + \rho_L g\tau\}\epsilon = (F_{PL})_{\text{liquid-filled}} \tag{3}$$

and for a gas-filled operation

$$\{(-dP/dZ)_{\text{gas-filled bed}} + \rho_G g\tau\}\alpha = (F_{PG})_{\text{gas-filled}} \tag{4}$$

According to Pironti et al. (1999), the wetting efficiency can be calculated as the ratio of the solid–liquid drag force (F_{PL}) in two-phase flow to that in liquid-filled bed at the same liquid flow rate. So

$$\eta = (F_{PL})_{\text{2-phase flow}}/(F_{PL})_{\text{liquid-filled}} \tag{5}$$

Similarly, the fraction of area that is not wetted by the liquid can be determined from the ratio of solid–gas drag force in two–phase flow to that in gas–filled bed at the same gas flow rate

$$1-\eta = (F_{PG})_{\text{2-phase flow}}/(F_{PG})_{\text{gas-filled}} \tag{6}$$

From Eqs. 1 and 2 after combining Eqs. 5 and 6 we get

$$\eta = \frac{\left[2F_I + (F_{PG})_{\text{gas-filled}} + \epsilon\{\rho_L g\tau + (-dP/dZ)\} - \epsilon\alpha\{g\tau + 2(-dP/dZ)\}\right]}{(F_{PL})_{\text{liquid-filled}} + (F_{PG})_{\text{gas-filled}}} \tag{7}$$

where $(-dP/dZ)$ is the two-phase pressure-drop.

Strategy for the Estimations of the Parameters

The following steps were followed for the estimation of the different parameters involved in Eq. 7.

(1) The gas–liquid interfacial drag force (F_I), tortuosity factor (τ), and two-phase pressure drop were calculated using the model of Narasimhan et al. (2002).

In the trickle-flow regime, the interfacial drag induced by the relative motion between the two phases can be modeled using the modified Kozeny-Carman equation, which is as follows

$$F_I = \epsilon(1-\alpha)\left(a'\mu_G V_r - b'\rho_G V_r^2\right) \tag{8}$$

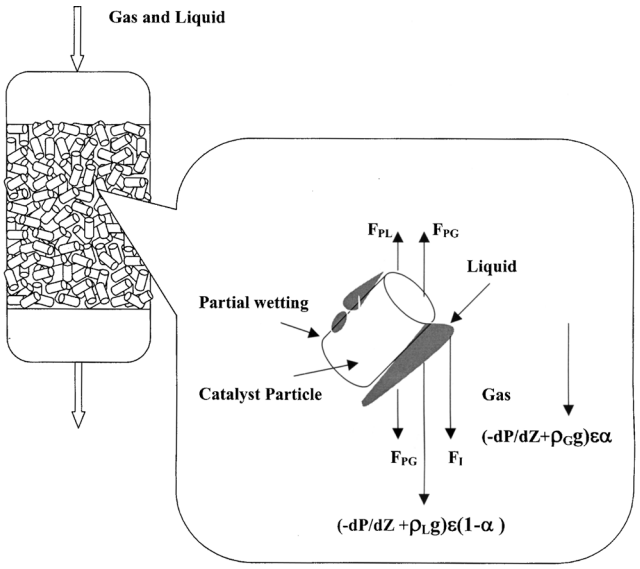

Figure 1. Model presentation and different types of forces acting during the flow of gas and liquid over the catalyst particle in a trickle-bed reactor.

where a' and b' are modified Ergun constants with the correction for the increase in particle volume due to the liquid layer, yielding an effective particle diameter of $[(1-\epsilon\alpha)/(1-\epsilon)]^{1/3}d_p$ and effective porosity, $\epsilon\alpha$. So

$$a' = a/\alpha^3\left[(1-\epsilon\alpha)/(1-\epsilon)\right]^{4/3}$$

$$\text{and} \qquad b' = b/\alpha^3\left[(1-\epsilon\alpha)/(1-\epsilon)\right]^{2/3} \tag{9}$$

V_r is the slip velocity, which accounts for the slip between the two phases

$$V_r = V_G - \left[\alpha/(1-\epsilon)V_L\right] \tag{10}$$

For the bubble flow regime, the gas–liquid interfacial drag, F_I, had been calculated by developing an expression for the drag on a single bubble/slug and then multiplying it by the number of bubbles/slugs per unit volume of the porous layer. The expression is

$$F_I^* = F_I/\left[g\epsilon(\rho_L - \rho_G)\right] = \frac{C_v' V_L V_s}{gD_b^2(1-\rho^*)\epsilon} + \frac{C_I'(1-\alpha+\rho^*\alpha)V_s}{gD_b(1-\rho^*)\epsilon^2} \tag{11}$$

where V_s is the drift velocity of the bubble relative to the mixture, given by

$$V_s = \left[V_G(1-\alpha)/\alpha\right] - V_L \tag{12}$$

The coefficients C_V' and C_I' depend on the flow regime prevailing. A detailed derivation of these, along with the mathematical modeling of the flow regimes, is given in Tung and Dhir (1988).

The tortuosity corrects the gravity term in Eqs. 1 and 2. It is defined as

$$\tau = \cos\theta - \mu\sin\theta \tag{13}$$

where tortuosity angle, θ, and friction factor, μ, are expressed in terms of liquid and gas superficial velocities. De-

Table 1. Physical Characteristics of Catalyst Used and Values of E_1 and E_2 for Single-Phase Flow in Ergun Equation

Type of Catalyst	Particle Size (m)	Equivalent Dia., d_P (m)	Bulk Dens. (kg/m^3)	Porosity (cm^3/g)	Surface Area (m^2/g)	Bed Void Fraction	E_1	E_2
Alumina spheres	0.003	0.003	750	0.185	285	0.36	250	2.1
Alumina tablet	0.00635x 0.00635	0.0073	800	0.5	215	0.42	167	1.8
Alumina holed tablet	0.006x 0.006 x0.002	0.0052	800	0.36	185	0.48	155	1.6
Alumina extrudates	0.00159	0.0045	550	0.4	210	0.47	225	1.9
Alumina trilobe (CDS)	0.00127	0.0034	500	0.5	235	0.53	155	1.7

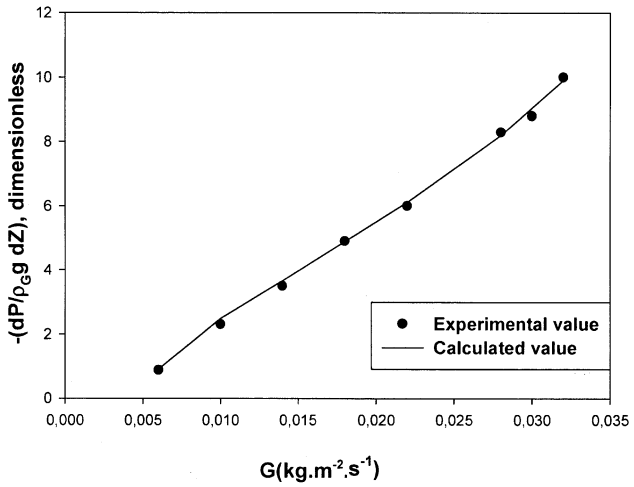

Figure 2. Experimental value of dimensionless pressure gradient in single-phase flow (only air) with alumina sphere as a catalyst particle and calculated values from Ergun equation with the value of $E_1 = 250$ and $E_2 = 2.1$.

tailed explanations are given in Narasimhan et al. (2002). The extra length traveled by the liquid due to the backmixing effect has also been considered in the tortuosity factor term.

(2) Equations 3 and 4 are used, respectively, for the estimation of the particle–liquid drag force in the liquid–filled operation and particle–gas drag force in a gas-filled operation. For getting the value of single-phase pressure drop for each phase, that is, $(-dP/dZ)_{\text{liquid-filled bed}}$ and $(dP/dZ)_{\text{gas-filled bed}}$, the Ergun equation is used

$$(-dP/dZ) + \rho_\alpha g = \frac{E_1 \mu_\alpha (1-\epsilon)^2 V_\alpha}{\epsilon^3 d_P^2} + \frac{E_2 \rho_\alpha (1-\epsilon) V_\alpha^2}{\epsilon^3 d_P} \tag{14}$$

where the subscript α is denoted for each phase (that is, gas and liquid). The constants E_1 and E_2 are calculated from the experiments with single-phase flow for each type of catalyst particle. The experimentally obtained values of E_1 and E_2 for each type of catalyst particle are reported in Table 1. These constants are obtained from the regression analysis of the experimental data. The experimentally obtained value and its predicted value with the value of $E_1 = 250$ and $E_2 = 2.1$ of the spherical catalyst has been shown in Figure 2.

(3) Two phase pressure drop is calculated from the combination of Eqs. 1 and 2 and the expression for the particle–gas drag, particle–liquid drag, and the gas–liquid interfacial drag (details in Narasimhan et al., 2002).

(4) Wetting efficiency is calculated from the experimental results based on the approach of Al-Dahhan and Dudukovic (1995). From the impulse response of the radioactive tracer, the first moment μ_1 and the variance, σ^2 are calculated numerically. According to the equation given in Al-Dahhan and Dudukovic (1995), the apparent effective diffusivity for the reactor in two-phase flow, $(De)_{TF}$, and in liquid-filled operation, $(De)_{LF}$, are obtained from the variance of the impulse response. The square root of the ratio of $(De)_{TF}$ and $(De)_{LF}$ will give the external wetting efficiency. For the calculation of $(De)_{LF}$, total liquid holdup (ϵ_L) is required, and is estimated from the first moment (μ_1) of the impulse response. Figure 3 shows the variation of total liquid holdup with superficial liquid-mass velocity at a constant superficial gas-mass

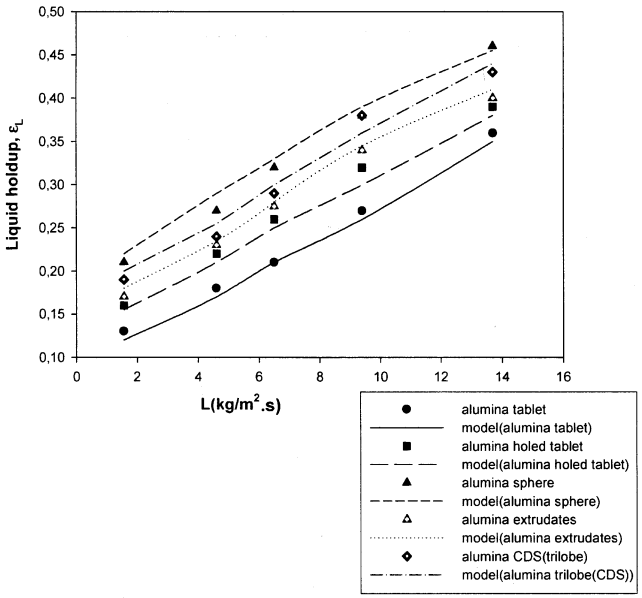

Figure 3. Experimental value of total liquid holdup from tracer studies and its prediction by the model of Narasimhan et al. (2002) ($G = 0.022$ kg/m^2·s).

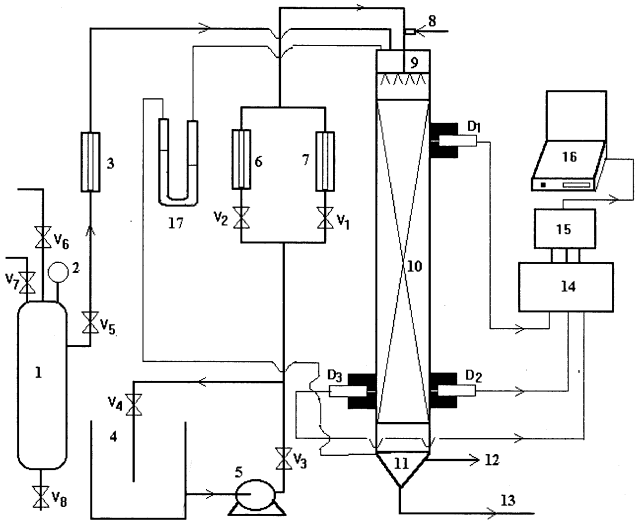

Figure 4. Experimental setup.

1: surge tank; 2: pressure gauge; 3: air rotameter; 4: water tank; 5: liquid feed pump; 6, 7: liquid rotameters; 8: tracer injection port; 9: liquid distributor; 10: trickle-bed reactor; 11: gas–liquid separator; 12: air outlet; 13: liquid outlet; 14: counter; 15: data-acquisition system; 16: PC; 17: manometer; D_1, D_2, D_3: collimated radiation detectors; $V_1 \cdots V_8$: valves.

velocity. The figure also shows the prediction of total liquid holdup ($G = 0.022\ \mathrm{kg \cdot m^{-2} \cdot s^{-1}}$) by the model of Narasimhan et al. (2002). Because the radioisotope tracer experiments are not an intrusive method, the moments (μ_1 and σ^2) are calculated directly from the response signal.

Experimental Setup

The experimental setup for the radioisotope tracer experiment in a trickle-bed reactor of 0.0152 m dia. is depicted in Figure 4. The experiments were carried out with five different types of packings with air–water flow at ambient conditions (temperature = 293 K and atmospheric pressure). The physical characteristics of the catalysts are given in Table 1. The operating range of liquid and gas in this study is 1.56–13.7 $\mathrm{kg \cdot m^{-2} s^{-1}}$ and 0.01–0.033 $\mathrm{kg \cdot m^{-2} s^{-1}}$, respectively. The liquid stored in a tank was continuously pumped into the column from the top through a distributor mounted 0.1 m above the packing. The liquid distributor consists of a stainless-steel tube of diameter 6.4×10^{-3} m, to which tubes of a dia. of 3.2×10^{-3} m were attached. There were 37 holes of size 1.5×10^{-3} m arranged in a square pitch of 2.0×10^{-2} m. ^{99m}Tc (half life: 6 h and gamma energy 0.14 MeV (87%) as sodium pertechnatate) was used as a tracer. ^{99m} Tc was extracted from the ^{99}Mo/^{99m}Tc-generator, and about 10–20 MBq activity was used in each run. The tracer was injected instantaneously into the inlet feed line through an injection port at the top of the column using a calibrated glass syringe. The tracer was injected after achieving steady-state flow. The tracer movement was monitored at the inlet (D_1) and outlet (D_2) of the column using collimated thallium-activated sodium iodide scintillation detectors separated by a distance of 1.25 m. In order to investigate the radial distribution of liquid, an additional detector, D_3, was mounted diametrically opposite to detector D_2 at the reactor outlet. The detectors were connected to a multichannel date-acquisition system (DAS). It is supposed that the number of counts measured by the detectors is proportional to the tracer concentration, C_t. The DAS was set to record 1,000 data points at an interval of 0.2 s. The tracer concentration was recorded until the radiation level at the outlet comes to the background level. The recorded data were transferred to the computer for subsequent analysis.

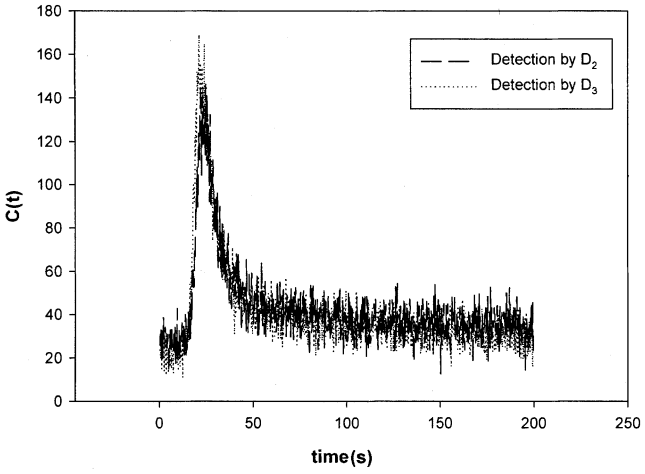

Figure 5. Typical tracer-response: (a) detected by D_2 and D_3 sensors with alumina sphere as a catalyst particle ($L = 6$ kg/m^2·s and $G = 0.022$ kg/m^2·s); (b) after the treatment detected by D_2 sensor with alumina sphere as a catalyst particle ($L = 6$ kg/m^2·s and $G = 0.022$ kg/m^2·s).

Results

The experimental response curve of the concentration of the radioisotope tracer of two dectectors, D_2 and D_3, are almost the same for all catalyst packings except alumina CDS (trilobe) and alumina extrudates. This corresponds to no significant radial maldistribution for the other three types of catalyst packings, that is, alumina sphere, alumina tablet and

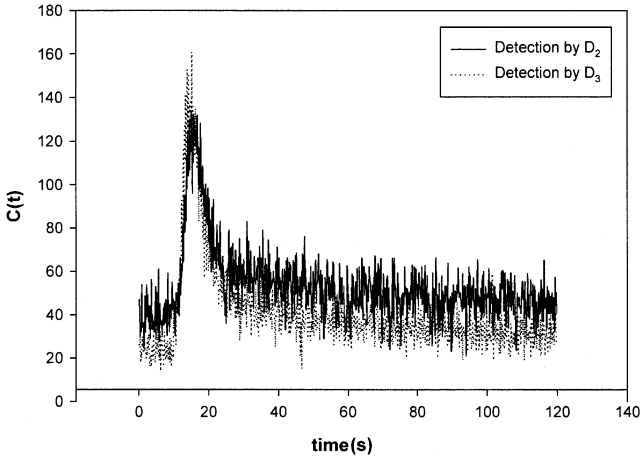

Figure 6. Typical tracer-response detected by D_2 and D_3 sensors with alumina extrudates as a catalyst particle ($L = 6$ kg/m^2·s and $G = 0.022$ kg/m^2·s).

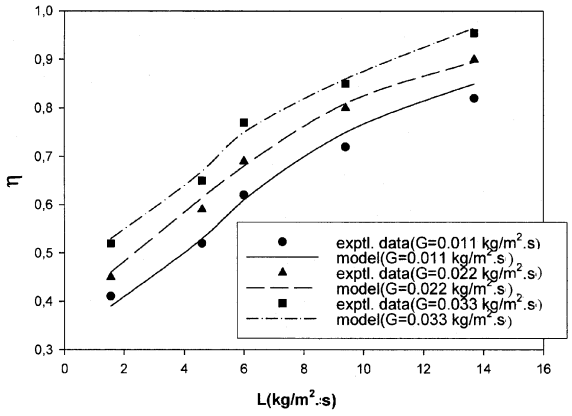

(a)

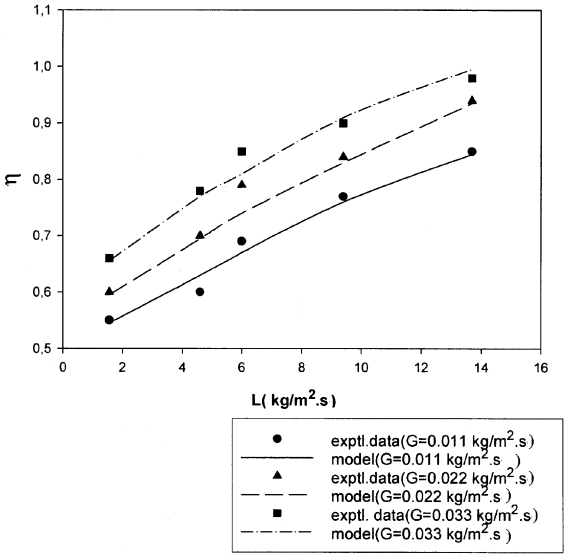

(b)

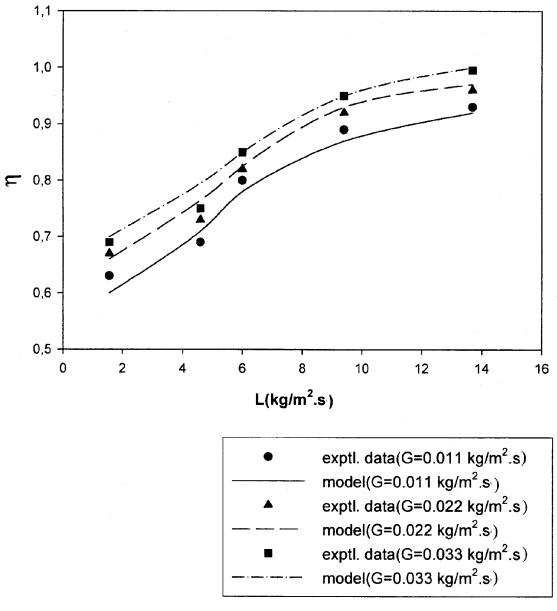

(c)

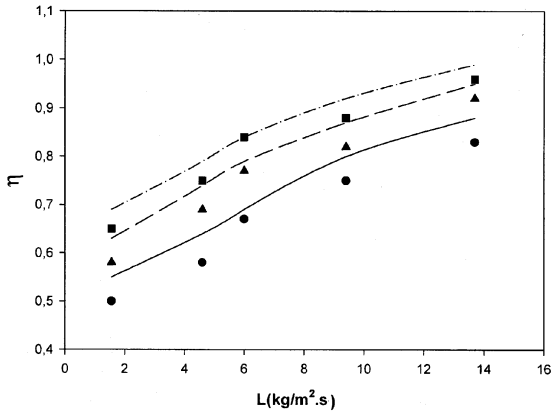

(d)

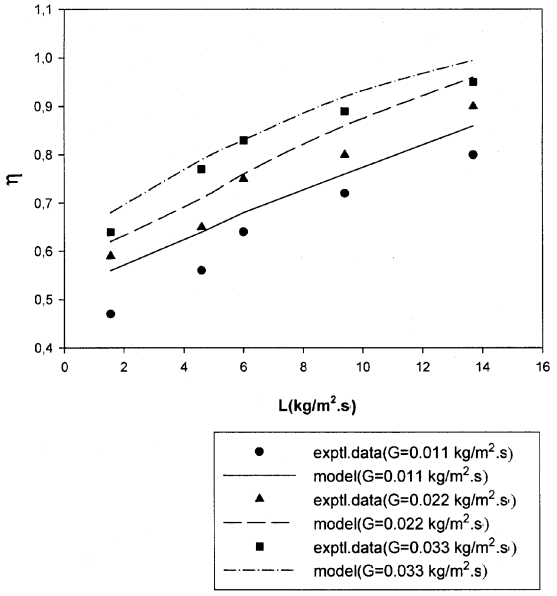

(e)

Figure 7. Wetting efficiency vs. superficial liquid-mass velocity at different superficial gas-mass velocities (a) experiment alumina holed tablet at a catalyst particle vs. models prediction; (b) experiment with alumina tablet as a catalyst particle vs. model's prediction; (c) experiment with alumina sphere as a catalyst particle vs. model's prediction; (d) experiment with alumina extrudates as a catalyst particle vs. model's prediction; (e) experiment with alumina trilobe (CDS) as a catalyst particle vs. model's prediction.

alumina holed tablet (see Figure 5a for alumina sphere), whereas for alumina CDS (trilobe) and alumina extrudates, a considerable radial maldistribution is observed (see Figure 6 for alumina extrudates). For the case of these two catalyst packings, an average of variance has been taken for the estimation of the wetting efficiency. About the calculation of second moment, the obtained experimental data (Figure 5a) have been treated to take into account the background subtraction, zero shifting, and tail correction. Figure 5b shows the resultant curve from which the value of the second moment was computed. A similar methodology has been used in the literature for such a response curve (Stegowski and Leclerc 2002; Pant et al., 2001).

Figures 7a–7e show the effect of superficial gas- and liquid-mass velocity on the wetting efficiency for five types of catalyst packing. It has a significant variation with higher superficial gas-mass velocity and negligible variation with a lower superficial gas-mass velocity at the same liquid load, which is similar to the observations of Al-Dahhan and Dudukovic (1995) and Pironti et al. (1999). This is due to the increase in pressure drop with the increase of superficial gas-mass velocity, which results in a decrease in liquid holdup and liquid film thickness. Consequently, there is an improvement of the spreading of the liquid over the catalyst which results in an increase in wetting efficiency. In the lower range of superficial gas-mass velocity, the effect of its variation on the pressure drop is very small. As expected, wetting efficiency increases with the increase of liquid load at a constant gas flow rate due to the increase in pressure drop and liquid holdup. Wetting efficiency is highest for spherical catalyst due to it being uniform in structure. Wetting efficiency is lowest with holed tablets, in which the high value of the surface area per volume of catalyst may be responsible. The comparatively low value of wetting efficiency with alumina extrudates and alumina CDS (trilobe) is due to the bypassing of the liquid, which is also confirmed by the response curve of the tracer concentration.

Figures 7a–7e also show the prediction of the wetting efficency of the five different catalyst packings by the present model. It predicts very well with the spherical catalyst and tablet. Although a considerable amount of maldistribution of liquid is present with the alumina extrudates and alumina CDS (trilobe), the prediction is within a range of $\pm 15\%$, which may be due to the inclusion of tortuosity in the model. The predictions of the model have been compared with the high-pressure experimental results of Al-Dahhan and Dudukovic (1995) for wetting efficiency in Figures 8a and 8b. The model is able to predict the influence of the operating pressure quite well. Figure 9 compares the data of wetting efficiency with the inert diluent (Al-Dahhan and Dudukovic, 1996), at high pressure, where large backmixing is possible. Pironti et al. (1999) have presented some experimental data of wetting efficiency derived from the pressure drop and liquid holdup measurements. The predictions of the model with the data of Pironti et al. (1999) are shown in Figure 10. Although, at low Reynolds number (up to $Re_G = 89$, $G = 0.26$ kg/m^2·s), the model predicts quite well, the prediction is within $\pm 23\%$ at high Reynolds number ($Re_G = 107$, $G = 0.31$

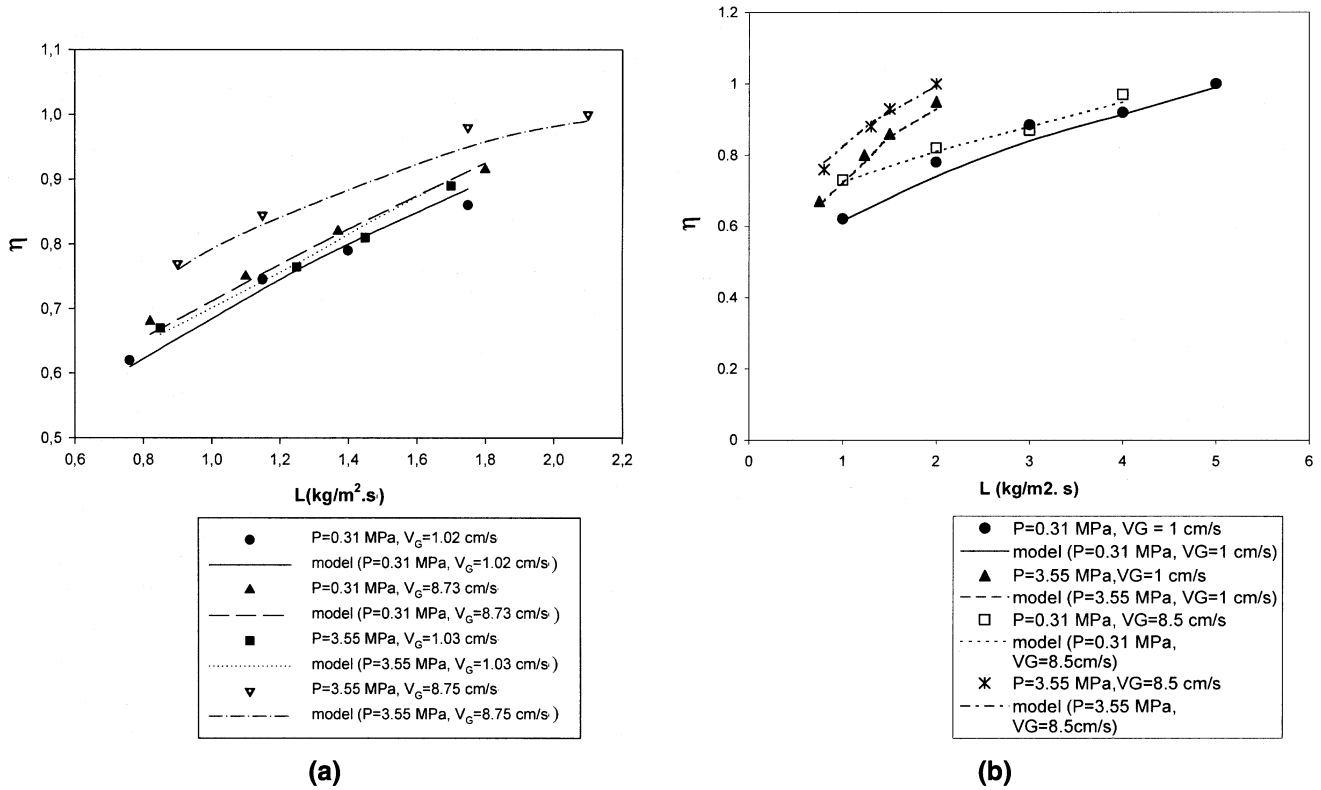

Figure 8. Theoretical predictions of wetting efficiency vs. experimental results of Al-Dahhan and Dudukovic (1995): (a) porous extrudates in hexane–nitrogen system at high pressure; (b) porous sphere in hexane–nitrogen system at high pressure.

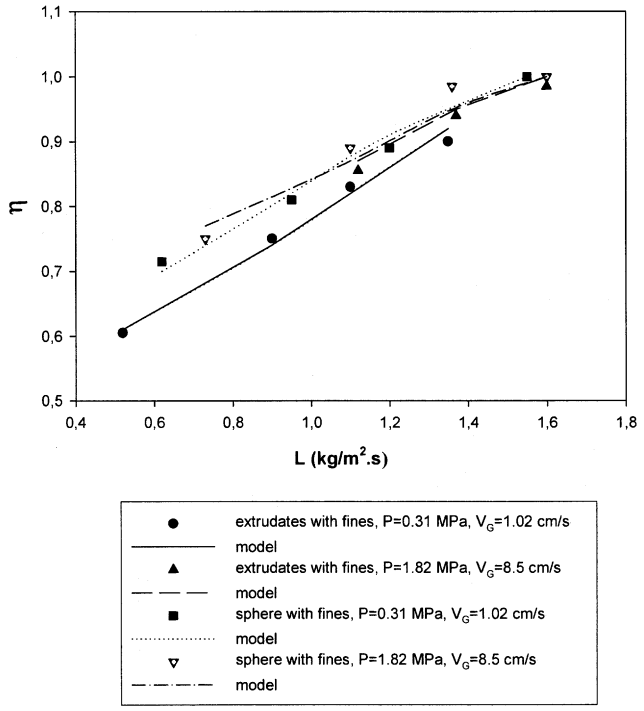

Figure 9. Theoretical predictions of wetting efficiency vs. experimental results of Al-Dahhan and Dudukovic (1996) in hexane–nitrogen system with dilution of the catalyst bed at high pressure.

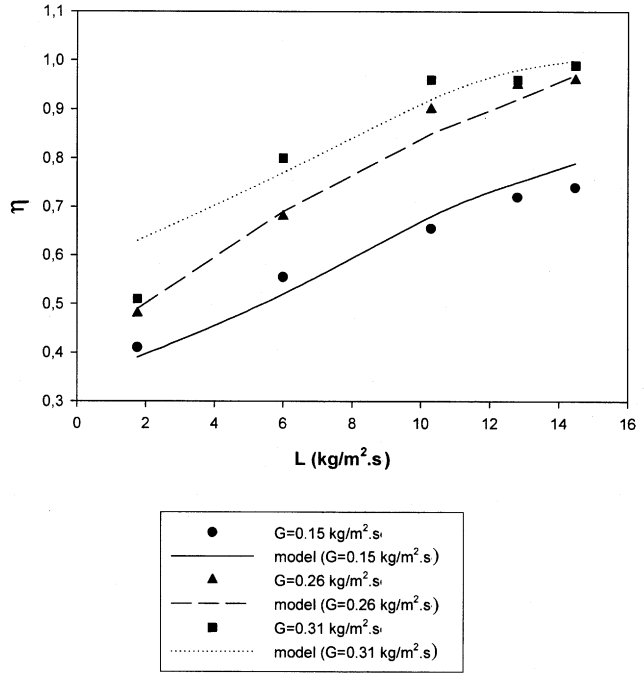

Figure 10. Theoretical predictions of wetting efficiency vs. experimental results of Pironti et al. (1999) in air–water system.

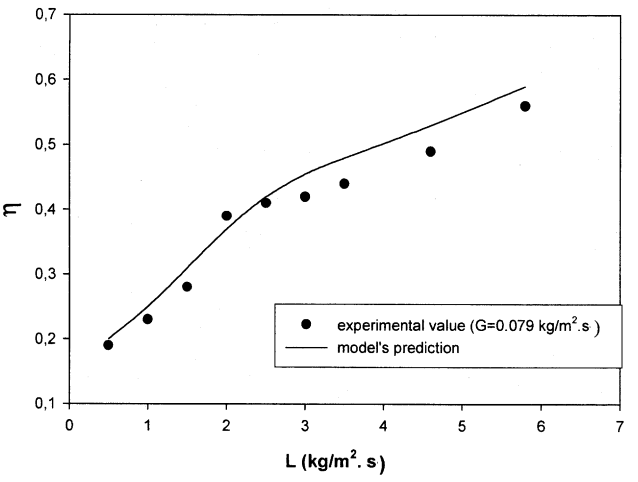

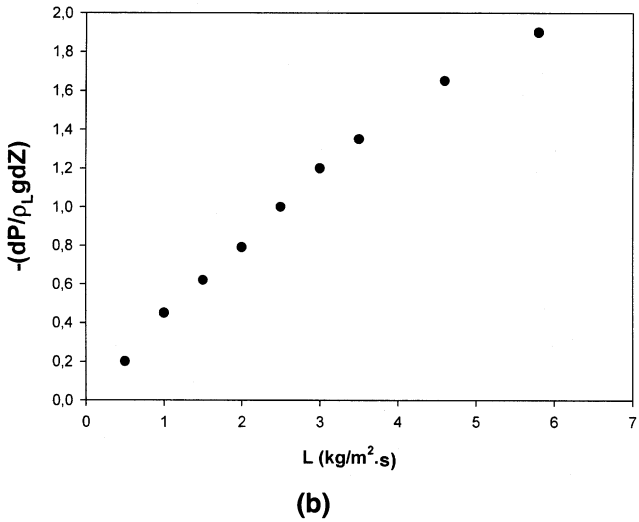

Figure 11. Theoretical predictions of wetting efficiency vs. experimental results of Sederman and Gladden (2001) in air–water system; (b) pressure-drop data predicted by the model of Narasimhan et al. (2002) for the system of Sederman and Gladden (2001).

kg/m^2·s). The gas–liquid interaction may play a significant role at this Re_G. Pressure drop for liquid-filled and gas-filled operation has been calculated from Ergun equations with the constants reported by the respective authors. The model also has been compared with the experimental results of wetting efficiency using magnetic-resonance imaging by Sederman and Gladden (2001). Figure 11a shows the prediction of wetting efficiency with the data of Sederman and Gladden (2001). The model predicts well up to a superficial liquid mass velocity of 2.5 kg·m^{-2}·s^{-1} and overestimates up to some extent at higher superficial liquid-mass velocity. It also has been observed that the present model overestimates the liquid saturation data by 18% of the findings of these authors. For a calculation of the wetting efficiency, the value of two-phase pressure drop is required and estimated using the model of Narasimhan et al. (2002). The prediction of pressure drop in

Table 2. Literature from Which Experimental Data are Taken

Authors	Systems	Operating Condition
Al-Dahan and Dudukovic (1995)	Hexane–nitrogen Porous sphere: $d_p = 0.00199$ m, $\epsilon_p = 0.599$, $\epsilon = 0.355$ Extrudate: $d_p = 0.00152$ m, $\epsilon_p = 0.697$, $\epsilon = 0.412$ $\rho_L = 633$ kg/m^3	$L = 0.42$–$2.7\ 10^{-3} - 4.03$ kg/m$^2\cdot$s $G = 6.64\times10^{-3}$–4.03 kg/m$^2\cdot$s $P = 0.31$–5.0 MPa, $T = 298$ K
Al-Dahhan and Dudukovic (1996)	Hexane–nitrogen, $\rho_L = 633$ kg/m^3 Extrudate: $d_p = 0.00152$ m, $\epsilon_p = 0.697$, $\epsilon = 0.412$ Vol. of fines/vol. of catalyst = 0.54, $\epsilon_{Bf} = 0.22$, $\epsilon_B = 0.38$ Vol. of fines/vol. of catalyst = 2, $\epsilon_{Bf} = 0.35$, $\epsilon_B = 0.77$ Porous sphere: $d_p = 0.00199$ m, $\epsilon_p = 0.599$, $\epsilon = 0.355$ Vol. of fines/vol. of catalyst = 0.4, $\epsilon_{Bf} = 0.31$, $\epsilon_B = 0.42$	$L = 0.42$–$2.7\ 10^{-3} - 4.03$ kg/m$^2\cdot$s $G = 6.64\times10^{-3}$–4.03 kg/m$^2\cdot$s $P = 0.31$–5.0 MPa, $T = 298$ K
Pironti et al. (1999)	Air–water $d_p = 0.00368$ m, $\epsilon = 0.25$, $\rho_L = 1{,}000$ kg/m^3	$L = 1.76$–14.48 kg/m$^2\cdot$s $G = 0.1$–0.31 kg/m$^2\cdot$s $P = 0.1$ MPa
Sederman and Gladden (2001)	Air–water Glass sphere: $d_p = 0.005$ m, $\epsilon = 0.43$, $\rho_L = 1{,}000$ kg/m^3	$L = 0.5$–5.8 kg/m$^2\cdot$s $G = 0.08$–0.43 kg/m$^2\cdot$s $P = 0.1$ MPa

their operating range is shown in Figure 11b. For the calculation of single-phase pressure drop, E_1 and E_2 are taken as 850 and 2, respectively, for the glass sphere from Holub et al. (1993). Table 2 summarizes all of the literature, from which the experimental data of wetting efficiency are compared with the present model. Figure 12 shows the parity plot of all the experimental data from the present experiment and the literature. Almost all data are bounded by $\pm 15\%$.

Conclusion

A model for the external wetting efficiency of catalyst in trickle-bed reactors has been developed. The model is based on the fundamental point-force balance, and incorporates particle–gas drag, particle–liquid drag, and gas–liquid interactions. The tortuosity effect has also been considered. The pressure drop and liquid holdup were predicted from the model of Narashiman et al. (2002), and were required for the evolution of wetting efficiency. Thus, it is a nonintrusive method for the prediction of external wetting efficiency. Experimental results are presented with five different types of catalyst packing with different geometry. The radioisotope tracer technique was used to collect the experimental data. The wetting efficiency of alumina extrudates and alumina CDS (trilobe) is smaller than that of the alumina sphere and holed tablet. Liquid maldistribution may be the reason. The model predicts with a reasonable accuracy using our experi-

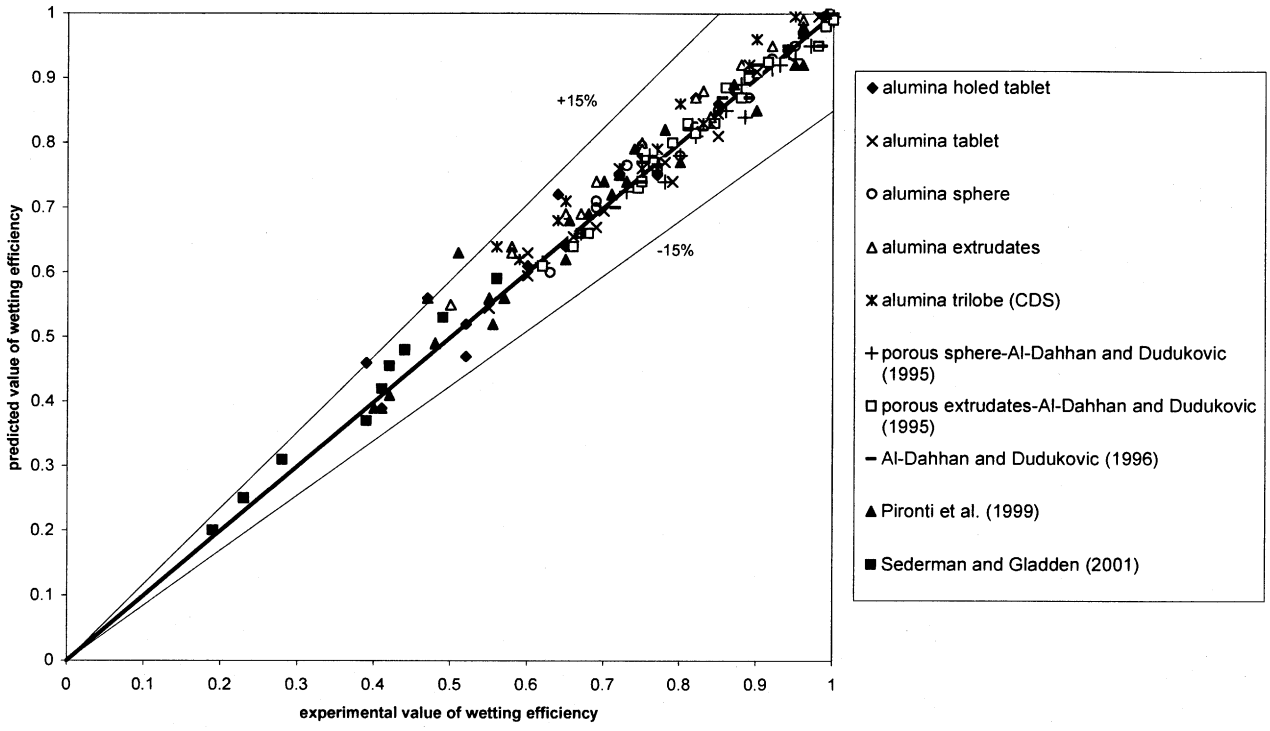

Figure 12. Parity plot for the prediction of wetting efficiency using this model.

mental results and the results reported in the literature. The mean relative error is 0.09.

Notation

C_I = inertial drag coefficient
C_t = concentration at time t s, mole·m^{-3}
C_V = viscous drag coefficient
d_P = particle diameter, m
D_b = bubble diameter, m
D_e = effective diffusivity, m^2/s
E_1, E_2 = Ergun constant for the single-phase flow on the packing
F_I = liquid–gas interfacial drag, kg·m^{-2}s^{-2}
F_I^* = dimensionless liquid–gas interfacial drag, $F_I/[g\epsilon(\rho_L - \rho_G)]$
F_{PG} = particle–gas drag, kg·m^{-2}s^{-2}
F_{PL} = particle–liquid drag, kg·m^{-2}s^{-2}
g = gravitational acceleration, m/s^2
G = superficial gas mass velocity, (kg·m^{-2}s^{-1})
L = superficial liquid mass velocity, kg·m^{-2}s^{-1}
V_s = drift velocity of bubble relative to the mixture, m/s
V = superficial velocity, m/s

Greek letters

α = gas saturation
β = liquid saturation
ϵ = porosity of packed bed
ϵ_L = liquid holdup
ϵ_p = particle porosity
η = wetting efficiency
μ = model friction factor
μ_G = viscosity of the gas phase, kg/m·s
μ_L = viscosity of the liquid phase, kg/m·s
ν_L = kinematic viscosity of liquid, m^2·s^{-2}
ρ_G = density of the gas phase, kg·m^{-3}
ρ_L = density of the liquid phase, kg·m^{-3}
ρ^* = dimensionless density, $\rho^* = \rho_L/\rho_G$
θ = inclination angle, rad
τ = tortuosity factor

Literature Cited

Al-Dahhan, M. H., and M. P. Dudukovic, "Catalyst Wetting Efficiency in Trickle-Bed Reactors at High Pressure," *Chem. Eng. Sci.*, **50**(15), 2377 (1995).

Al-Dahhan, M. H., and M. P. Dudukovic, "Catalyst Bed Dilution for Improving Catalyst Wetting in Laboratory Trickle-Bed Reactors," *AIChE J.*, **42**(9), 2594 (1996).

Chander, A., A. Kundu, S. K. Bej, A. K. Dalai, and D. K. Vohra, "Hydrodynamic Characteristics of Cocurrent Upflow and Downflow of Gas and Liquid in a Fixed Bed Reactor," *Fuel,* **80**, 1043 (2001).

Holub, R. A., M. P. Dudukovic, and P. A. Ramachandran, "A Phenomenological Model for Pressure Drop, Liquid Holdup, and Flow Regime Transition in Gas-Liquid Trickle Flow," *Chem. Eng. Sci.*, **47**, 2343 (1992).

Holub, R. A., M. P. Dudukovic, and P. A. Ramachandran, "Pressure Drop, Liquid Holdup, and Flow Regime Transition in Trickle Flow," *AIChE J.*, **39**, 302 (1993).

Iliuta, I., F. Larachi, and B. R. A. Grandjean, "Catalyst Wetting in Trickle-Bed Reactors: A Phenomenological Model," *Chem. Eng. Res. Des.*, **77**, 759 (1999).

Iliuta, I., and F. Larachi, "The Generalized Slit Model: Pressure Gradient, Liquid Holdup and Wetting Efficiency in Gas-Liquid Trickle Flow," *Chem. Eng. Sci.*, **54**, 5039 (1999).

Kundu, A., A. K. Saroha, and K. D. P. Nigam, "Liquid Distribution Studies in Trickle-Bed Reactors," *Chem. Eng. Sci.*, **56**, 5963 (2001).

Larachi, F., L. Belfares, and B. P. A. Grandjean, "Prediction of Liquid-Solid Wetting Efficiency in Trickle Flow Reactors," *Int. Comman. Heat Mass Transfer*, **28**(5), 595 (2001).

Llano, J. J., R. Rosal, H. Sastre, and F. V. Diez, "Determination of Wetting Efficiency in Trickle-Bed Reactors by a Reaction Method," *Ind. Eng. Chem. Res.*, **36**, 2616 (1997).

Mills, P. L., and M. P. Dudukovic, "Evaluation of Liquid-Solid Contacting in Trickle Bed Reactors by Tracer Methods," *AIChE J.*, **27**, 893 (1981).

Narasimhan, C. S. L., R. P. Verma, A. Kundu, and K. D. P. Nigam, "Modeling Hydrodynamics of Trickle-Bed Reactors at High Pressure," *AIChE J.*, **48**, 2459 (2002).

Nigam, K. D. P., A. K. Saroha, A. Kundu, and H. J. Pant, "Radioisotope Tracer Study in Trickle-Bed Reactors," *Can. J. Chem. Eng.*, **79**, 860 (2001).

Pant, H. J., A. Kundu, and K. D. P. Nigam, "Radiotracer Applications in Chemical Process Industry," *Rev. Chem. Eng.*, **17**(3), 165 (2001).

Pironti, F., D. Mizrahi, A. Acosta, and D. Gonzalez-Mendizabal, "Liquid–Solid Wetting Factor in Trickle-Bed Reactors: Its Determination by a Physical Method," *Chem. Eng. Sci.*, **54**, 3793 (1999).

Ring, Z. E., and R. W. Missen, "Trickle-Bed Reactors. Tracer Study of Liquid Holdup and Wetting Efficiency at High Pressure and Temperature," *Can. J. Chem. Eng.*, **69**, 1016 (1991).

Rucker, C. M., and A. Akgerman, "Determination of Wetting Efficiencies for a Trickle-Bed Reactor at High Temperatures and Pressures," *Ind. Eng. Chem. Res.*, **26**, 164 (1987).

Sederman, A. J., and L. F. Gladden, "Magnetic Resonance Imaging as a Quantitative Probe of Gas-Liquid Distribution and Wetting Efficiency in Trickle-Bed Reactors," *Chem. Eng. Sci.*, **56**, 2615 (2001).

Saroha, A. K., and K. D. R. Nigam, "Trickle Bed Reactor," *Rev. Chem. Eng.*, **12**, 207 (1996).

Sicardi, S., G. Baldi, V. Specchia, I. Mazzarino, and A. Geianetto, "Packing Wetting in Trickle Bed Reactors: Influence of the Gas Flow Rate," *Chem. Eng. Sci.*, **36**, 226 (1980).

Sie, S. T., and R. Krishna, "Process Development and Scale Up: III. Scale-Up and Scale-Down of Trickle Bed Processes," *Rev. Chem. Eng.*, **14**, 203 (1998).

Stegowski, Z., and J.-P. Leclerc, "Determination of the Solid Separation and Residence Time Distributions in an Industrial Hydrocyclone Using Radioisotope Tracer Experiments," *Int. J. Miner. Process.*, **66**, 67 (2002).

Tung, V. X., and V. K. Dhir, "A Hydrodynamic Model for Two Phase Flow Through Porous Media," *Int. J. Multiphase Flow*, **14**, 47 (1998).

Appendix

Let us consider the 0.152-m-dia. trickle-bed reactor with spherical catalyst particles ($d_p = 0.003$ m, internal porosity = 0.185) and a bed porosity of 0.36 operating in the trickle-flow regime. The process variables are $V_L = 0.0046$ m/s and $V_G = 0.0182$ m/s at a temperature of 293 K and atmospheric pressure. The liquid is water (density = 1,000 kg/m^3 and viscosity = 0.00001 kg/m·s), and the gas is air (density = 1.207 kg/m^3 and viscosity = 0.0000183 kg/m·s).

1. Calculation of gas saturation, α and two-phase pressure-drop.

(a) Liquid-phase force balance

$$\left[\frac{-dP}{dZ} + \rho_L g\tau\right](1-\alpha)\epsilon = F_{PL} - F_I \qquad \text{(A)}$$

(b) Gas-phase force balance

$$\left[\frac{-dP}{dZ} + \rho_G g\tau\right]\alpha\epsilon = F_{PG} + F_I \qquad \text{(B)}$$

The dimensionless form of Eq. B is

$$P^*\alpha = \frac{-\rho^*\alpha\tau}{(1-\rho^*)} + F^*_{PG} + F^*_I \qquad \text{(C)}$$

and the dimensionless form of Eq. A is

$$P^*(1-\alpha) = \frac{-(1-\alpha)\tau}{(1-\rho^*)} + F^*_{PL} - F^*_I \qquad \text{(D)}$$

where

$$P^* = \frac{-\frac{dP}{dZ}}{g(\rho_L - \rho_G)}, \qquad \rho^* = \frac{\rho_G}{\rho_L}$$

$$\text{and} \qquad F^* = \frac{F}{g\epsilon(\rho_L - \rho_G)}$$

(c) Model for F^*_{PG}

$$F^*_{PG} = \frac{a^*\mu_G V_G}{\kappa_G} + \frac{b^*\rho_G V_G^2}{\eta_G} \qquad \text{(E)}$$

where

$$a^* = \frac{a}{g(\rho_L - \rho_G)} \qquad \text{and} \qquad b^* = \frac{b}{g(\rho_L - \rho_G)}$$

$$\kappa_G = \left(\frac{1-\epsilon}{1-\epsilon\alpha}\right)^{4/3}\alpha^2 \qquad \text{and} \qquad \eta_G = \left(\frac{1-\epsilon}{1-\epsilon\alpha}\right)^{2/3}\alpha^2$$

(d) Model for F^*_{PL}

$$F^*_{PL} = \frac{a^*\mu_L V_L}{\kappa_L} + \frac{b^*\rho_L V_L^2}{\eta_L} \qquad \text{(F)}$$

where $\kappa_L = \eta_L = (1-\alpha)^3$

(e) Model for F^*_I

$$F^*_I = \frac{(1-\alpha)}{\alpha}\left(\frac{a^*\mu_G V_r}{\kappa_G} + \frac{b^*\rho_G V_r^2}{\eta_G}\right) \qquad \text{(G)}$$

where

$$V_r = V_G - \frac{\alpha}{1-\alpha}V_L$$

(f) Model for τ: The tortuosity factor has been calculated using the equation

$$\tau = \cos\theta - \mu\sin\theta \qquad \text{(H)}$$

where

$$\theta = \Pi/2[1 - e^{K(V_L+V_G)}] \qquad \text{and} \qquad \mu = (K_1 - K_2)/(V_L + V_G)$$

The models for particle–gas drag, particle–liquid drag, and the liquid–gas interfacial drag (Eqs. E, F, and G) with the model for tortuosity are now used in conjunction with the force balances on the liquid and gas phases (Eqs. C and D) to predict the liquid saturation and pressure drop. Elimination of the pressure gradient between the two dimensionless force-balance equations (Eqs. C and D) yields the following nonlinear equation

$$\alpha(1-\alpha)\tau + F^*_{PG}(1-\alpha) - \alpha F^*_{PL} + F^*_I = 0 \qquad \text{(I)}$$

where α is calculated using the Newton-Raphson algorithm.

$$\eta = \frac{\left[2F_I + (F_{PG})_{\text{gas-filled}} + \epsilon\{\rho_L g\tau + (-dP/dZ)\} - \epsilon\alpha\{g\tau + 2(-dP/dZ)\}\right]}{(F_{PL})_{\text{liquid-filled}} + (F_{PG})_{\text{gas-filled}}}$$

For the preceding case, we get $\alpha = 0.417$, from which we obtain the value of $\beta_t = 1 - 0.417 = 0.583$ and $h_L = \epsilon\beta_t = 0.36 \times 0.583 = 0.21$.

2. Calculation of wetting efficiency: The equation for the calculation of wetting efficiency

(a) Once we get the value of α, the pressure drop can be calculated using Eq. C or D.

(b) F_I is calculated using Eq. G.

(c) τ has been determined from Eq. H.

(d) $(F_{PG})_{\text{gas-filled}}$ and $(F_{PL})_{\text{liquid-filled}}$ are calculated using Eqs. 3 and 4 in the text.

(e) The value of $(-dP/dZ)_{\text{liquid-filled bed}}$ and $(dP/dZ)_{\text{gas-filled bed}}$ required for the evaluation of $(F_{PG})_{\text{gas-filled}}$ and $(F_{PL})_{\text{liquid-filled}}$ are estimated using the Ergun equation (Eq. 14) ($E_1 = 250$ and $E_2 = 2.1$).

Manuscript received May 28, 2002, and revision received Feb. 11, 2003.